Vol. 77, No. 21

Spatial Variations in Archaeal Lipids of Surface Water and Core-Top Sediments in the South China Sea and Their Implications for Paleoclimate Studies[▽][†]

Yuli Wei,[1] Jinxiang Wang,[1,2] Jie Liu,[1] Liang Dong,[1] Li Li,[1]* Hui Wang,[1] Peng Wang,[1] Meixun Zhao,[3] and Chuanlun L. Zhang[1,4]*

State Key Laboratory of Marine Geology, Tongji University, Shanghai 200092, China[1]; School of Earth Resources, China University of Geosciences-Wuhan, Wuhan 430074, China[2]; Institute of Marine Organic Geochemistry, Ocean University of China, Qingdao 266100, China[3]; and Department of Marine Sciences, University of Georgia, Athens, Georgia 30602[4]

The South China Sea (SCS) is the largest marginal sea of the western Pacific Ocean, yet little is known about archaeal distributions and TEX_{86}-based temperatures in this unique oceanic setting. Here we report findings of abundances in both core lipids (CL) and intact polar lipids (IPL) of *Archaea* from surface water (CL only) and core-top sediments from different regions of the SCS. TEX_{86}-derived temperatures were also calculated for these samples. The surface water had extremely low abundances of CL (average of 0.05 ± 0.13 ng/liter; $n = 75$), with higher values present in regions where upwelling is known to occur. The core-top sediments had CL values of 0.1 to 0.9 μg/g, which are on the low end of CL concentrations reported for other marine sediments and may reflect the oligotrophic nature of the open SCS. The IPL of *Archaea* accounted for 6 to 36.4% of total lipids (CL plus IPL), indicating that the majority of archaeal lipids in core-top sediments were derived from nonliving cells. The TEX_{86}-based temperatures of surface water were overall lower than satellite-based sea surface temperatures or CTD-measured *in situ* temperatures. The core-top sediment samples, however, had TEX_{86} temperatures very close to the mean annual sea surface temperatures, except for samples with water depths of less than 100 m. Our results demonstrated low and heterogeneous distributions of archaeal lipids in surface water and core-top sediments of the SCS, which may reflect local or regional differences in productivity of *Archaea*. While TEX_{86}-based temperatures for core-top marine sediments at deep water depths (>100 m) generally reflected mean annual sea surface temperatures, TEX_{86} temperatures in surface water varied basin wide and underestimated sea surface temperatures in most locations for the season when surface water samples were collected.

The ocean contains a daunting number of *Archaea*, which amount to approximately 10^{28} cells (30). This huge biomass, however, was unaccounted for 20 years ago and has attracted increasing attention to the roles of these organisms in carbon and nitrogen cycles in the global ocean (see, e.g., references 13, 25, and 49). One unique aspect of *Archaea* is their membrane lipids, which are sensitive to temperature variations and have been used to develop paleotemperature proxies (31, 32, 55). Planktonic *Archaea* are also known to participate in ammonia oxidation, thus playing an important role in the nitrogen cycle in the ocean (49).

The South China Sea (SCS) is the largest marginal sea of the western Pacific Ocean and belongs to the "East Indies Triangle," which is the center of the maximum species diversity within the world's largest biogeographic region, the tropical Indo-West Pacific (6). The basin of the SCS is characterized by oligotrophic conditions, a shallow mixed layer and nutricline, low primary production (41), and low export production (8).

The climatic system of the SCS is affected by the proximity to the Tibetan Plateau and Pacific warm pool and characterized by the East Asian monsoons. As a result, the SCS is one of the best places for paleoclimate studies. Furthermore, the SCS has the most suitable conditions for high-resolution paleoceanographic studies because of high sedimentation rates and good carbonate preservation (64). The SCS is also highly suitable for examining the relationships between continental weathering, productivity, and climate, as three of the largest rivers in the world (from north to south, the Pearl River, the Red River, and the Mekong River) provide detrital fluxes to the basin of the SCS (61).

Numerous paleoclimate studies have been conducted in the SCS, which are commonly based on temperature proxies such as oxygen isotope ratios and Mg/Ca ratios of foraminifera, foraminiferal transfer function, or the U_{37}^{K} methods (27, 28, 67). It has been realized that individual temperature proxies all can suffer from some biases (2), and the ideal approach would be the integration of multiple proxies for addressing the same question (12). The TEX_{86} proxies have been developed only recently (31, 32, 55) and most successfully used for marine systems (see, e.g., references 5, 7, 11, and 43). In terrestrial environments, the TEX_{86} proxies have been successfully applied to paleoclimate studies of some large lakes (4, 51, 52).

Despite the importance of the SCS in studies of primary

---

* Corresponding author. Mailing address: State Key Laboratory of Marine Geology, Tongji University, Shanghai 200092, China. Phone: 86-21-65982215. Fax: 86-21-65988808. E-mail for Li Li: lilijxj@yahoo.com.cn. E-mail for Chuanlun Zhang: archaea.zhang@gmail.com.
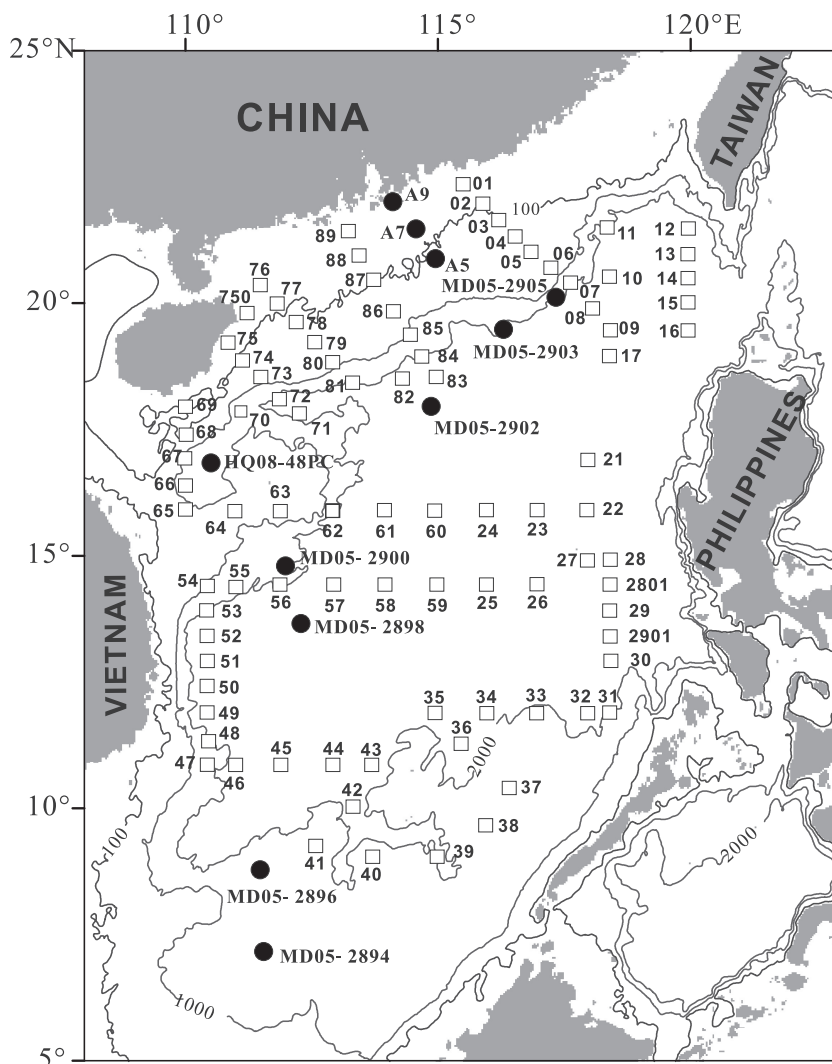
FIG. 1. Map showing stations at which surface water was collected (open squares) and locations where sediment cores were collected (solid circles) in the South China Sea. (Adapted from reference 64a with kind permission from Springer Science+Business Media.)

production and paleoclimate, little research has been done regarding the abundance and community structure of *Archaea* and the application of archaeal lipids as temperature proxies in the SCS. In this study, we performed archaeal and bacterial glycerol dibiphytanyl glycerol tetraether (GDGT) analyses of both the core lipids (CL) and intact polar lipids (IPL) from both surface water and core-top sediments of the SCS. Our data for the core-top sediments from water depths of greater than 100 m showed that TEX_{86}-derived sea surface temperatures (SST) based on CL matched annual mean sea surface temperatures from the satellite data, whereas TEX_{86}-derived sea surface temperatures based on surface water samples collected in April and May 2010 were lower than satellite-based or CTD-determined sea surface temperatures for those months. This study is the first calibration between satellite sea surface temperatures and TEX_{86}-derived temperatures in the SCS, which may provide a reference for studies of paleoclimate changes in the SCS using these proxies.

MATERIALS AND METHODS

Sample collections. (i) Water column sampling. A cruise in the SCS was made on 23 April to 26 May 2010 by using the R/V *Shiyan No. 3* of the South China Sea Institute of Oceanology, Chinese Academy of Sciences. A total of 89 sampling stations were visited (Fig. 1), among which 78 stations were sampled for archaeal lipids from the surface water (5- to 10-m water depths). At each location, filtration of seawater was conducted using a submersible pump, which was connected to a filtration system that contained three parallel and identical glass fiber filters (142-mm diameter) with the same pore size (0.7 μm). The total volume of water for all three filters was recorded, and the filters were collected using sterile stainless steel forceps into 50-ml sterile Falcon tubes. The tubes were immediately stored in a −20°C freezer on board the R/V *Shiyan No. 3* after collection, transported under ambient temperature within 3 h, and stored at −80°C until further analysis.

(ii) Core-top sediment sampling. Sediment samples were collected using coring devices during three cruises in the SCS (Fig. 1). Cores A9, A7, and A5 were retrieved in July 2009 using the R/V *Dongfanghong No. 2*, core HQ08-48PC was collected in 2008 using the R/V *Haiyang No. 4*, and cores MD05-2894 to MD05-2905 were obtained during the Chinese-French joint Marco Polo/Images 147 cruise in 2005 using the R/V *Marion-Dufresne*. The lengths of these cores were less than 10 m. On board, the cores were opened and subsamples for lipid and microbiological studies were taken from the centers of the cores under sterile

conditions and stored in airtight sterile PVC tubes in a $-20°C$ freezer. Subsamples for chemical measurements were taken from the core, packed with aluminum foil, and then stored in cloth bags in a $-20°C$ freezer. Only the core-top sediments (<5-cm depths) were used for this study.

Concentration and isotopic compositions of TOC. About 5 g of sediment was decarbonated using 10% HCl and neutralized by repeated washing with distilled and deionized water before analysis. Part of the dried bulk sediment was used for analysis of total organic carbon (TOC). The concentrations of TOC were determined with an EA1110 organic element analyzer (Carlo Erba). The carbon isotopes of the TOC were then determined on a GV-Isoprime EA IRMS with a precision of 0.1‰ for $\delta^{13}C$ (referenced to the Vienna Pee Dee Belemnite [VPDB]), which is defined as $\delta^{13}C = [(^{13}C/^{12}C)_{sample}/(^{13}C/^{12}C)_{standard} - 1] \times 1,000$.

Lipid analyses. (i) Lipid extraction and fractionation. Three methods were used for extraction of total lipids. In all three methods, the original sample was spiked with an internal standard (C_{46}, 974.08 ng) before the extraction procedure began. Method A was used for core HQ08-48PC. In this method, the freeze-dried sediment sample spiked with the internal standard was extracted ultrasonically five times with a mixture of dichloromethane (DCM) and methanol (MeOH) (3:1, vol/vol). The total extract was transferred into a KOH-MeOH solution (6%), left overnight, and then extracted with n-hexane five times. Method B was used for cores A9, A7, and A5. The freeze-dried sediment sample was ultrasonically extracted three times with MeOH, three times with DCM-MeOH (1:1, vol/vol), and three times with DCM, and all extracts were combined. Method C was used for all filter samples, which produced core lipid only. In this method, the freeze-dried filter material was cut into small pieces using sterilized scissors and then put into a 40-ml tube. MeOH, MeOH-DCM (1:1, vol/vol), and DCM were used to extract lipids from the filter material sequentially, with each step repeated at least once. Extract from each step was collected, and the total extract was transferred into a KOH-MeOH solution (6%), left overnight, and extracted with n-hexane five times (22).

The final extract obtained from each method was fractionated into apolar and polar fractions using the same procedure. Briefly, the total extract was poured into a glass pipette column filled with activated silica gel and sequentially eluted with hexane-DCM (9:1, vol: vol) to obtain the apolar fraction and with DCM-MeOH (1:1, vol/vol) to obtain the polar fraction. To obtain the core GDGTs (C-GDGTs), the polar fraction was filtered through a 0.45-μm polytetrafluoroethylene (PTFE) filter and directly injected onto a liquid chromatograph-mass spectrometer (LC-MS). The intact polar GDGTs (IP-GDGTs) were indirectly obtained as described by Huguet et al. (22). Briefly, half of the polar fraction was dried under N_2 and hydrolyzed with 5% (vol/vol) HCl in MeOH for 4 h at 70°C. The hydrolyzed GDGT fractions were sequentially extracted four times with DCM–Milli-Q water (1:1) and four times with Milli-Q water after hydrolysis was complete. Each extraction was followed by centrifugation, and all extracts were pooled into one sample. The extracts were dried under N_2 and dissolved in 300 μl n-hexane–isopropanol (99:1, vol/vol) before analysis by LC-MS. The IPL were calculated as the difference between the yields after and before hydrolysis (22).

(ii) GDGT analysis and quantification. Analyses of GDGTs were performed at Tongji University by a slightly modified method of Schouten et al. (56). Separation was performed using an Agilent 1200 liquid chromatograph equipped with an automatic injector and a Prevail Cyano column (2.1 by 150 mm, 3 μm; Alltech, Deerfield, IL), maintained at 40°C. The GDGTs were first eluted isocratically with n-hexane and isopropanol as follows: 99% n-hexane and 1% isopropanol for 5 min and then a linear gradient to 1.8% isopropanol in 45 min. The flow rate was 0.2 ml/min. After each analysis, the column was cleaned by back flushing n-hexane–isopropanol (90:10, vol/vol) at 0.2 ml/min for 10 min. Detection was performed using an Agilent 6460 triple-quadrupole mass spectrometer (MS) with an atmospheric pressure chemical ionization (APCI) ion source. Conditions for APCI MS were as follows: nebulizer pressure, 60 lb/in^2; vaporizer temperature, 400°C; drying gas (N_2) flow, 5 liters/min; temperature, 200°C; capillary voltage, -3.5 kV; corona, 5 μA (3.2 kV). The single-ion monitoring (SIM) mode was used to detect eight isoprenoidal and branched GDGT signals (m/z 1302, 1300, 1298, 1296, 1292, 1050, 1036, and 1022), one diether signal (m/z 653), and the C_{46} internal standard (m/z 744), with a dwell time of 237 ms per ion. The analytical error for TEX$_{86}$ determined by replicate analysis was better than ±0.008 for all samples, which corresponded to about $\pm0.4°C$ according to Kim et al. (31).

(iii) Calculations of GDGT proxies. TEX$_{86}$ and TEX$_{86}^H$ were calculated as follows (32, 55): TEX$_{86}$ = (GDGT-2 + GDGT-3 + GDGT-5′)/(GDGT-1 + GDGT-2 + GDGT-3 + GDGT-5′) and TEX$_{86}^H$ = log[(GDGT-2 + GDGT-3 + GDGT-5′)/(GDGT-1 + GDGT-2 + GDGT-3 + GDGT-5′)]. TEX$_{86}$-derived sea surface temperatures (SST) were calculated according to three different equations. Equation 1 is from Schouten et al. (55), who originally used a limited

number of core-top samples. Equation 2 is from Kim et al. (31), who updated the proxy of Schouten et al. (55) using an extended number of samples globally.

$$T = 66.7 \times \text{TEX}_{86} - 18.67 \qquad (1)$$

$$T = 56.2 \times \text{TEX}_{86} - 10.78 \qquad (2)$$

The third equation is according to Liu et al. (43): $T = 50.47 - 16.33/\text{TEX}_{86}$.

Kim et al. (32) also developed an equation (equation 3) which is suitable for the reconstruction of SST in nonpolar oceans:

$$\text{SST} = 68.4 \times \text{TEX}_{86}^H + 38.6 \qquad (3)$$

where TEX$_{86}^H$ is the logarithmic function of TEX$_{86}$. This equation was also used to calculate sea surface temperatures from core-top samples in the SCS.

A ring index (RI) was calculated for both CL and IPL as described by Pearson et al. (50): RI = [(% GDGT-1) + 2 $\times$ (% GDGT-2) + 3 $\times$ (% GDGT-3) + 4 $\times$ (% GDGT-4) + 5 $\times$ (% GDGT-cren) + (% GDGT-cren-isomer)]/100.

Another proxy used in this study is the BIT (branches isoprenoidal tetraethers), which defines the input of terrestrial organic matter to the ocean (17): BIT = (I + II + III)/(I + II + III + GDGT-5).

(iv) Statistical analysis. Cluster analyses were performed using the relative abundances of archaeal GDGTs to evaluate the relationships among lipid compositions. The dendrogram of the cluster analysis was constructed with the R programming language software (freeware available at http://cran.r-project.org/ [44]) using Euclidean distance measure and ward linkage.

(v) Satellite data. The satellite-derived SST were obtained from the best SST (bSST) data sets from the NOAA advanced very-high-resolution radiometer (AVHRR) (version 5.0; http://pathfinder.nodc.noaa.gov) on a 4-km spatial resolution. For the core-top sediment samples, we extracted and averaged the annual mean bSST for the 5 years between 2004 and 2009 using MATLAB. For the surface water samples collected during April and May 2010, we used the mean surface temperature for the same months of 2009.

RESULTS

Basic physical/chemical conditions for surface water and surface marine sediments. The water depth ranged from 42 m to 4176 m for stations at which surface filter samples were collected (see Table S1 in the supplemental material). Water depths for core-top sediment samples ranged from 33 m to 3,697 m (Table 1). Water chemistry was not available for the filter samples, and pore water chemistry of the core-top sediments was determined only for the HQ core. The concentration of total organic carbon (TOC) ranged from 0.18% to 1.36%, with an average value of 0.94% $\pm$ 0.33% ($n = 11$). The $\delta^{13}C$ of TOC ranged from -19.54‰ to -24.2‰, with an average value of -21.21‰ $\pm$ 0.33‰ ($n = 11$), which is indicative of marine primary production (26, 46).

Abundances and distributions of archaeal lipids (CL and IPL). (i) Surface water samples. At each station, 200 to 1,100 liters of water was filtered. The abundances of total archaeal CL were all above the detection limit of the instrument (0.8 pg). However, 21 out of the 78 total filter samples gave very low yields based on the examination of the internal standard; these samples were eliminated from further analysis. The remaining samples showed total archaeal CL concentrations ranging from 0.001 ng/liter to 0.894 ng/liter of seawater (see Table S1 in the supplemental material). High values (concentrations above 0.1 ng/liter) were observed near Hainan Island and the east coast of Vietnam and in the central basin or the Bashi Strait between Taiwan and the Philippines; on the other hand, low archaeal CL concentrations commonly occurred in the southeast side of the SCS (Fig. 2). Overall, there is no correlation between concentrations of total archaeal CL and water column depths, as demonstrated by the presence of high values in waters of all

TABLE 1. General physical/chemical properties, total core lipids, and intact polar lipids, of archaea and bacteria of surface sediment samples from the South China Sea

Parameter	Value at station:										
	MD05-2894	MD05-2896	MD05-2898	MD05-2900	MD05-2902	MD05-2903	MD05-2905	HQ08-48PC	A5	A7	A9
Latitude (N)	07°02.25′	08°49.50′	13°47.39′	14°23.33′	17°57.70′	19°27.32′	20°08.17′	16°57.5134′	20°59.746′	21°30.199′	22°00.50′
Longitude (E)	111°33.11′	111°26.47′	112°11.03′	110°41.74′	114°57.33′	116°15.15′	117°21.61′	110°31.5809′	114°58.784′	114°30.040′	113°59.963′
Water depth (m)	1,982	1,657	2,395	1,455	3,697	2,066	1,647	1,474	102	73	33
Sand content (%)	0.3	0.0	0.6	0.0	5.8	0.4	0.7	0.0	10.7	3.3	1.5
Silt content (%)	70.2	70.7	74.3	77.3	75.5	76.7	82.4	82.1	79.3	82.0	80.1
Clay content (%)	29.5	29.3	25.1	22.7	18.7	22.9	16.8	17.8	10.1	14.7	18.3
Total organic carbon (%)	1.11	1.32	0.97	1.09	1.36	1.01	1.07	0.70	0.18	0.79	0.77
$\delta^{13}C_{org}$ (‰)	−20.78	−19.95	−19.59	−20.66	−20.53	−20.98	−21.05	−21.47	−24.20	−22.30	−21.80
Total archaeal CL (ng/g)	0.41	0.28	0.27	0.32	0.13	0.11	0.25	0.59	0.29	0.90	0.77
Total archaeal IPL (ng/g)	0.05	0.02	0.16	0.05	0.04	0.02	0.04	ND[a]	0.06	0.06	ND
Total branched CL (ng/g)	10.07	8.89	12.68	14.18	3.23	3.14	5.39	38.09	14.43	69.04	73.15
Total branched IPL (ng/g)	2.92	0.88	13.24	3.48	1.09	1.03	1.37	ND	4.41	17.79	ND

[a] ND, not determined.

depths (Fig. 3). The concentrations of branched tetraether lipids indicative of bacteria were generally below the detection limit in the filter samples and thus were not reported.

(ii) Sediment samples. In sediment samples, total archaeal CL ranged from 0.11 μg/g to 0.90 μg/g, with the highest value occurring in the shallow water depth (A7, 73 m) (Fig. 4). Total archaeal IPL ranged from 0.02 μg/g to 0.16 μg/g, with the highest value occurring at MD05-2896 of the deep water (Table 1). Similar to the case for the filter samples, high total
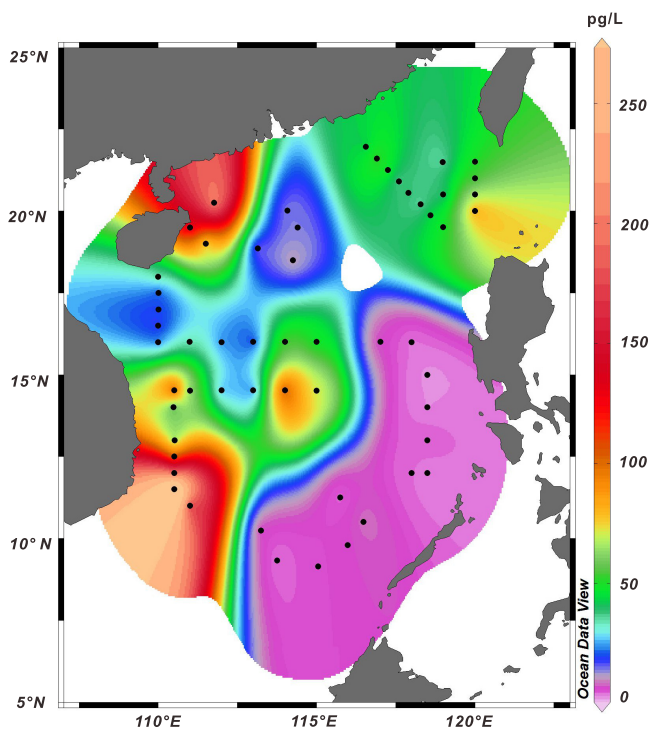

FIG. 2. Map showing the distribution of abundances of total archaeal core lipids from surface water of the South China Sea. (Map generated with Ocean Data View software.)

archaeal CL occurred in both shallow (<200-m) and deep (>1,000-m) waters, and the highest abundance also occurred in the shallower sediments (Fig. 4).

Total branched CL ranged from 3.14 ng/g to 38.72 ng/g, with the highest value occurring at the shallowest water depth (A9, 33 m) (Table 1). Total branched IPL ranged from 0.88 ng/g to 13.24 ng/g; the highest value occurred at the same location (MD05-2896) where the highest archaeal IPL occurred.

Relative abundances of GDGTs in CL and IPL. (i) Filter samples. GDGTs of archaeal CL were dominated by crenarchaeol (25.1% to 65.0%) and GDGT-0 (4.2 to 45.5%) (see Table S1 in the supplemental material). No archaeol (diether) (see Appendix for an explanation of structures) was detected in filter samples. Cluster analysis of the relative GDGT distributions showed no grouping of filter samples according to depth (Fig. 3), suggesting that water depth is unlikely to be a factor affecting the distribution of archaeal lipids in the surface water of the SCS.

(ii) Sediment samples. The highest abundances of archaeal GDGTs in either CL or IPL were also crenarchaeol (35.12 to 69.73%) and GDGT-0 (16.20 to 31.69%). For the same sample, crenarchaeol was consistently lower in relative abundance in IPL than in CL, whereas GDGT-0 was consistently higher in IPL than in CL. Archaeol was also higher in IPL than in CL in all but one sample (A7). Other GDGT compounds were either higher or lower in IPL than in CL; however, the majority of GDGT-2 and GDGT-3, and to a less extent, GDGT-1 and GDGT-4, showed higher values in IPL than in CL (Table 2). The ring index had a range of 2.28 to 3.70, with the IPL ring index being 0.20 to 1.37 units higher than the CL ring index (Table 2). However, there was no correlation between CL- and IPL-derived ring indices (data not shown), suggesting different GDGT compositions in the two lipid pools.

Cluster analysis showed that the compositions of the archaeal CL GDGTs at shallower (<100-m) water depths were different from those at water depths of below 1,000 m. Within the deep-water cluster, however, no spatial patterning was observed across the basin (Fig. 4). Comparison of the A9, A7, and
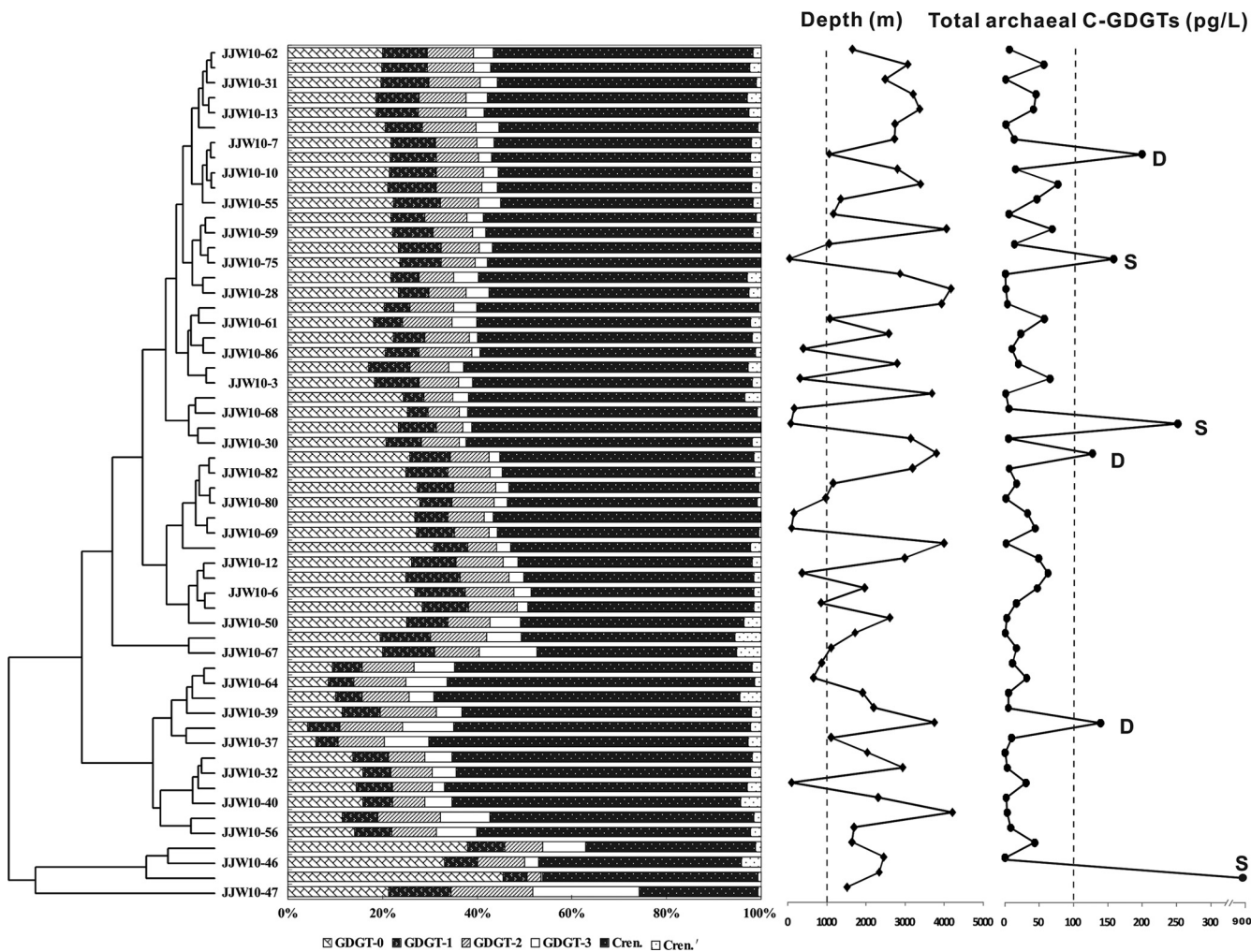
FIG. 3. Clustering analysis of relative abundances of glycerol dibiphytanyl glycerol tetraethers (GDGTs) in core lipids of *Archaea* from surface water of the South China Sea. Also plotted are water depths for stations where the surface water samples were collected and total core lipids of *Archaea* at each station. D, deep water (>1,000 m); S, shallow water (<1,000 m).

A5 sediment samples with filter samples at water depths near 100 m or below showed that the shallow-sediment C-GDGTs were more similar to those in water samples in the same region than to those farther away from it (data not shown), suggesting a possible local connection between core-top sediment GDGTs and those of the planktonic *Archaea*. The BIT was less than 0.2 for both CL and IPL at all water depths (Table 2), indicating minor contributions of terrestrial organic matter in these locations (17).

TEX$_{86}$-derived temperatures. (i) SST derived from surface water filter samples. Because the filter samples were collected during April and May of 2010, satellite-derived sea surface temperatures (SST) of April and May 2009 and CTD temperatures recorded during the sampling period were compared to TEX$_{86}$-derived temperatures. The satellite and CTD temperature maps were consistent in showing the generally higher sea surface temperature in the southern part (below the 17.5°N line) of the SCS than in the northern part; however, CTD temperatures to the east of Hainan Island were 2 to 4°C higher than the satellite temperatures (Fig. 5).

Comparison of satellite sea surface temperatures and the three calculation methods showed the best match for satellite SST averaged for April and May of 2009 and the calculation based on that described by Kim et al. (32) (see Table S1 in the supplemental material), whereas use of satellite-based mean annual SST showed a poorer correlation (data not shown). The majority of TEX$_{86}$ temperatures calculated according to the method of Kim et al. (32) were lower than satellite temperatures (Fig. 6A) or CTD temperatures (Fig. 6B). This was particularly evident in the northern SCS (Fig. 5). On average, the difference was 3.0 ± 2.3°C (n = 57) between satellite sea surface temperatures (averaged for April and May 2009) and TEX$_{86}$-derived temperatures and 3.4 ± 2.9°C (n = 57) between CTD and TEX$_{86}$ temperatures. The larger differences (e.g., greater than 5.0°C) between satellite sea surface temperatures and TEX$_{86}$ values occurred mostly outside the central basin and toward the land (e.g., samples 15, 30, 48, 69, 75, 76, and 85) (Fig. 1). The large differences between CTD and TEX$_{86}$ temperatures also occurred mostly at these stations (data not shown).
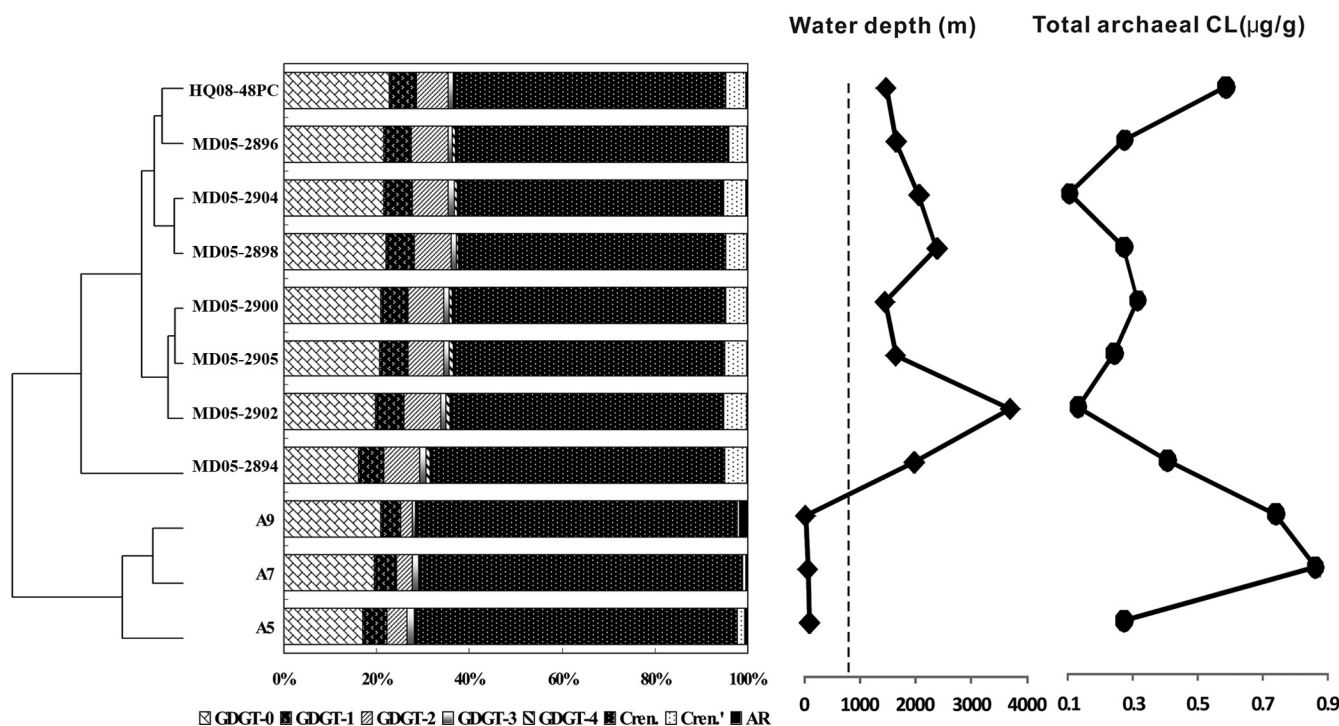
FIG. 4. Clustering analysis of relative abundances of glycerol dibiphytanyl glycerol tetraethers (GDGTs) in core lipids of *Archaea* from core-top sediments of the South China Sea. Also plotted are water depths at which core-top sediment samples were collected and total core lipids of *Archaea* at each station.

(ii) SST derived from core-top sediments. In most cases the TEX_{86}^{H}-derived temperatures based on IP-GDGTs were higher than those based on C-GDGTs (Table 2). In some cases, the difference between C-GDGT- and IP-GDGT-derived temperatures could be as large as 18.3°C according to the formula of Schouten et al. (55) (equation 1). This difference decreased when formulas of Kim et al. (31, 32) (equations 2 and 3) were used, and the latter formula (equation 3) gave the smallest difference between the C-GDGT- and IP-GDGT-derived temperatures (Table 2).

The TEX_{86} temperatures determined according to the method of Kim et al. (32) gave the closest match to the mean annual sea surface temperature from the satellite data. In the CL, the difference between satellite and TEX_{86} temperatures (32) was less than 1.0°C in all deep-water core-top sediments except MD05-2902, which had a difference of 1.1°C (Table 2). In core-top sediments from shallower water (A9, A7, and A5), however, the difference was considerably larger (4.3 to 9.2°C), with TEX_{86} temperatures lower than satellite temperatures (Fig. 7). Overall, the mean difference between mean annual satellite and TEX_{86} temperatures was 1.9 ± 2.4°C ($n = 11$), which was much smaller than differences observed for filter samples (note that the uncertainty of the calibration in use is 2.5°C, which is greater than the 1.9°C mean difference observed).

In the IPL of the deep-water samples, the difference between satellite and TEX_{86} temperatures (32) was mostly greater than 0.5°C, and it was up to 9.3°C in MD05-2896 (Table 2). Similar to the case for the CL, the IPL temperatures of the shallow-water core-top sediments gave larger differences from

the satellite values than those of the deeper-water core-top sediments (Table 2).

DISCUSSION

Abundance and distribution of GDGTs. (i) Filter samples. The average concentration of C-GDGTs (0.05 ± 0.13 ng/liter; $n = 57$) for all filter samples (see Table S1 in the supplemental material) was less than 10% of the average concentrations of C-GDGTs determined in other oceanic water column studies (16, 22, 59, 62, 63). Factors affecting the measured abundance of C-GDGTs in oceanic waters may include difference in methods of lipid extraction and different relative responses in the mass spectrometer, growth stage of the planktonic *Archaea*, seasonal variation in planktonic archaeal productivity, water column depth, and/or other variables. Huguet et al. (22) compared several extraction methods on both a living culture and environmental samples. They observed that the living culture had trace amounts of C-GDGTs, indicating that actively growing cells were composed mostly of IP-GDGTs. Environmental samples (including particles from the water column), on the other hand, had considerable amounts of C-GDGTs relative to IP-GDGTs, suggesting that large proportions of environmental lipids were derived from nonliving cells. Those authors also recommended using sonication or Soxhlet extraction for studies aiming to determine TEX_{86}-derived temperatures or to quantify the relative abundances of C- versus IP-GDGTs. Our study followed the sonication extraction method recommended by Huguet et al. (22), and the low concentrations of CL are unlikely to be due to method biases. Although we do not know

the growth stage of the planktonic *Archaea* in the SCS, estimates of lifetimes of planktonic *Archaea* are on the order of days to weeks (24). In reference to what Huguet et al. (21, 23) have observed, the low concentrations of C-GDGTs in our filter samples may not represent cells that were all active at the time of sampling. Another possible explanation for low GDGT concentrations may be the degradation of these compounds during transportation at ambient temperature. However, degradation, if any, appears not to have affected the calculation of temperatures based on the TEX$_{86}$ formula, which is consistent with Schouten et al. in that oxic degradation does not affect the TEX$_{86}$ values within the analytical error (54).

Depth distribution and/or seasonal variation in planktonic *Archaea* may be better reasons for the low concentrations of C-GDGTs in the surface water of the SCS. Quantification of archaeal biomass using molecular DNA methods has repeatedly shown that *Crenchaeota*, which are thought to be the major producers of GDGTs in the ocean, are at low levels in surface water and increase in relative or absolute abundances with depth (see, e.g., references 9, 30, 45, 47, and 65). A study of archaeal abundance in the SCS showed the same pattern, with surface water (5 m) having about 10^3 copies of archaeal 16S rRNA genes per ng of DNA, whereas at 75 m the archaeal abundance was 2 orders of magnitude higher (18). Depth profiles of archaeal lipids in the Black Sea also showed low GDGT concentrations in surface water (10 m) and a maximum at about the 100-m depth, which agrees with the maximum *Archaea* cell numbers (63). Similarly, in the Gulf of Mexico, GDGTs were detected at depths of 400 m and 869 m but not at 10 m (40). On the other hand, planktonic *Archaea* also vary in abundance in different seasons, with colder temperatures favoring a higher abundance of *Archaea* in many oceanic regimes (14, 16, 48, 65). It is possible that the low concentration of C-GDGTs in the SCS surface water resulted from sampling in a nonwinter season. This hypothesis has yet to be tested through seasonal and vertical sampling of the water columns in the SCS, which has been planned for the near future.

High abundances of planktonic *Archaea* are often found in association with upwelling and the oxygen minimum zone (OMZ) (1, 10, 33, 36). In the SCS, upwelling commonly occurs in regions northwest of Luzon and north of Sunda Shelf in winter and off the east coast of Vietnam in summer (41). The abundances of archaeal CL in surface water were indeed enhanced in these regions, particularly off the east coast of Vietnam (Fig. 2). However, we did not document whether upwelling was occurring during our sampling period, and such a cause-effect relation cannot be determined from our data. Also, the high abundance in the region between Hanan Island and the mainland may be related to upwelling over the widened northern SCS shelf, as indicated by model simulation and limited observations (15, 29). The OMZ commonly occurs below the sea surface, and it is unknown how surface (<10-m) archaeal populations may be affected by the OMZ below.

(ii) Sediment samples. The C-GDGTs in the sediment samples (Table 2) are at the lower end of the ranges observed in other marine sediment environments (see Table 4 in reference 22). For example, C-GDGTs in the range of 0.09 to 11 μg/g were reported for the Drammensfjord sediment in Norway (20, 23), C-GDGTs in the range of 0.06 to 195 μg/g for the Arabian Sea sediment (20), and C-GDGTs in the range of 0.02 to 7.73

TABLE 2. Relative abundances of GDGTs and archaeol in both core lipids and intact polar lipids of surface marine sediments in the South China Sea as well as TEX$_{86}$-based temperatures calculated according to different formulas, satellite mean annual sea surface temperatures, and BIT values

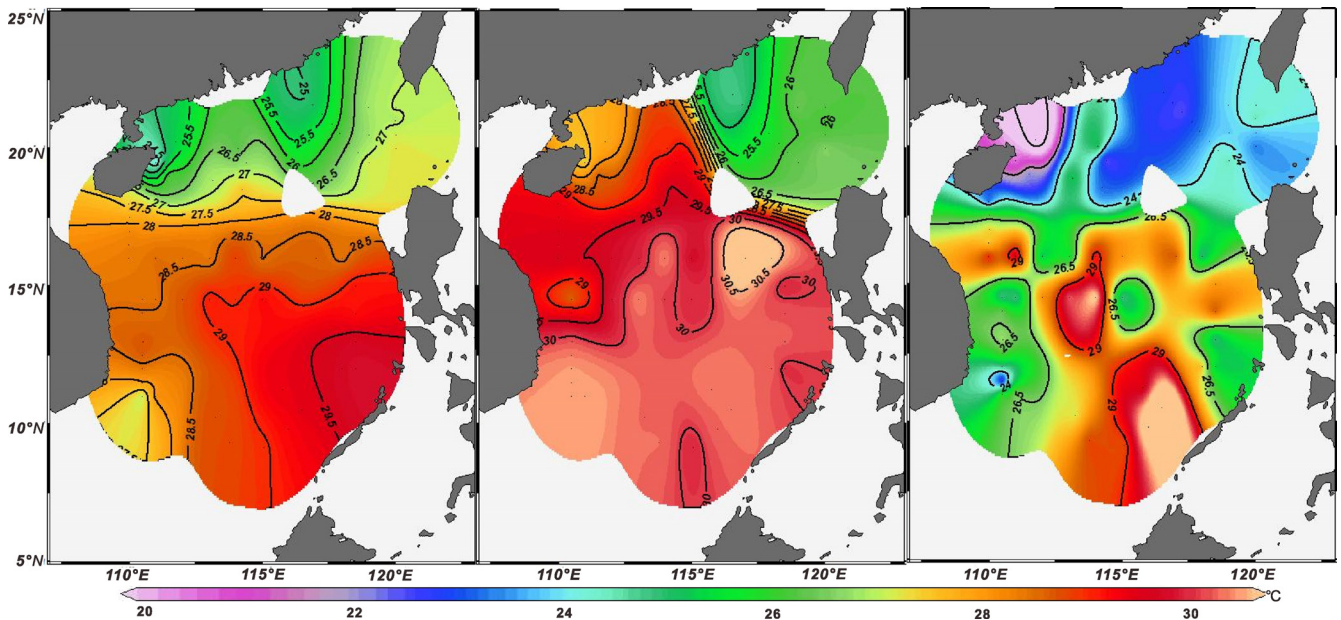| Sample	GDGT-0 (m/z 1302)	GDGT-1 (m/z 1300)	GDGT-2 (m/z 1298)	GDGT-3 (m/z 1296)	GDGT-4 (m/z 1294)	GDGT-5 (m/z 1292)	GDGT-5' (m/z 1292)	Archaeol (m/z 653)	Ring index	TEX$_{86}$	TEX$_{86}^H$	55	31	32	42	Satellite SST (°C)	BIT
	Relative abundance of archaeal lipids (%)											Temp (°C) determined according to reference:					
MD05-2894-CL	16.20	5.29	7.79	1.41	0.89	63.48	4.80	0.14	3.70	0.73	−0.14	29.71	30.00	29.08	27.97	28.49	0.03
MD05-2894-IPL	18.65	6.70	7.60	2.46	0.22	56.73	6.35	1.29	3.46	0.71	−0.15	28.68	29.13	28.43	27.48	28.49	0.08
MD05-2896-CL	21.61	5.82	7.98	0.97	0.60	58.92	3.92	0.18	3.41	0.69	−0.16	27.23	27.91	27.51	26.75	28.11	0.04
MD05-2896-IPL	27.79	0.31	1.05	1.98	0.35	57.11	5.24	6.16	3.22	0.96	−0.02	45.60	43.40	37.51	33.53	28.11	0.06
MD05-2898-CL	21.99	6.12	7.95	1.14	0.55	57.45	4.49	0.31	3.37	0.69	−0.16	27.30	27.97	27.56	26.79	28.11	0.06
MD05-2898-IPL	27.07	6.01	8.39	0.84	0.70	51.39	4.14	1.46	3.06	0.69	−0.16	27.30	27.99	27.62	26.80	27.68	0.12
MD05-2900-CL	20.82	5.98	7.61	1.15	0.66	58.96	4.60	0.23	3.45	0.69	−0.16	27.40	28.05	27.62	26.84	27.37	0.05
MD05-2900-IPL	31.69	7.61	10.35	1.99	3.99	35.12	4.31	6.53	2.46	0.73	−0.13	30.31	30.51	29.44	28.24	27.37	0.15
MD05-2902-CL	19.77	6.01	8.03	1.08	0.88	58.97	4.95	0.24	3.48	0.70	−0.16	27.83	28.42	27.90	27.06	26.66	0.03
MD05-2902-IPL	23.88	6.32	9.08	1.36	0.00	53.28	5.01	1.07	3.20	0.71	−0.15	28.66	29.12	28.42	27.47	26.66	0.04
MD05-2903-CL	21.46	6.24	7.72	1.20	0.69	57.47	4.82	0.41	3.39	0.69	−0.16	27.19	27.88	27.48	26.73	26.66	0.04
MD05-2903-IPL	29.32	6.01	7.62	1.34	2.21	47.87	4.16	1.47	2.94	0.69	−0.16	27.06	27.40	27.40	26.66	26.66	0.06
MD05-2905-CL	20.63	6.14	9.08	1.23	0.95	58.48	4.79	0.15	3.45	0.69	−0.16	27.34	28.00	27.58	26.80	26.82	0.03
MD05-2905-IPL	25.20	5.24	6.93	1.36	1.14	51.76	4.15	2.05	3.12	0.74	−0.13	28.00	30.40	29.49	28.28	26.82	0.05
HQ08-48PC-CL	22.76	5.72	5.72	1.00	0.00	58.93	4.22	0.45	3.38	0.68	−0.17	26.65	27.42	27.13	26.45	27.07	0.06
A5-CL	16.90	5.93	5.15	1.58	0.00	67.85	2.00	0.60	3.70	0.60	−0.23	21.04	22.69	23.21	23.05	26.40	0.03
A5-IPL	16.67	6.30	10.62	6.98	0.00	54.21	4.04	1.19	3.40	0.77	−0.11	32.97	32.75	31.01	29.39	26.40	0.08
A7-CL	19.34	5.45	3.95	1.35	0.00	68.31	1.13	0.47	3.65	0.54	−0.27	17.41	19.63	20.36	20.29	26.40	0.05
A7-IPL	18.82	19.70	19.21	7.91	0.00	21.77	7.41	5.17	2.28	0.64	−0.27	23.78	25.00	25.00	24.82	25.82	0.15
A9-CL	21.14	4.56	2.91	1.09	0.00	67.65	0.69	1.96	3.55	0.51	−0.29	15.15	17.73	18.44	18.28	25.64	0.07

FIG. 5. Maps of satellite-based average sea surface temperatures for the April-May season during which the surface water samples were collected (left), *in situ* temperatures determined from CTD (middle), and TEX$_{86}$-based temperatures of surface water samples according to reference 32. (Maps generated with Ocean Data View software.)

μg/g for Atlantic Ocean sediments (19). Lower C-GDGT abundance has been explained as being a result of an enhanced degradation rate under oxic conditions (19). It is unknown whether in this study differential degradation contributed to the lower C-GDGT concentrations in our surface marine sediments. On the other hand, the low GDGT concentrations may reflect the overall oligotrophic conditions of the South China Sea (41), which is consistent with the low C-GDGT concentrations in the surface water and supported by the relatively low TOC (average = 0.94 ± 0.12%, n = 11) in these samples (Table 1) (39).

IP-GDGTs accounted for 6.0 to 36.4% of total GDGTs (C plus IP). This is consistent with observations reported by others (20, 38, 42) and suggests that the majority of GDGT lipids in marine core-top sediments are derived from nonliving *Archaea*. The sources of CL and IPL in marine sediments, however, are debated and can come from either *in situ* production (3, 38, 39, 42) or possibly relict IPL from the water column (57). In particular, benthic archaeal populations seem to be able to recycle fossil GDGTs from planktonic *Archaea* (37, 42, 60), which can explain the higher TEX$_{86}$ temperatures based on IPL than on CL (42).
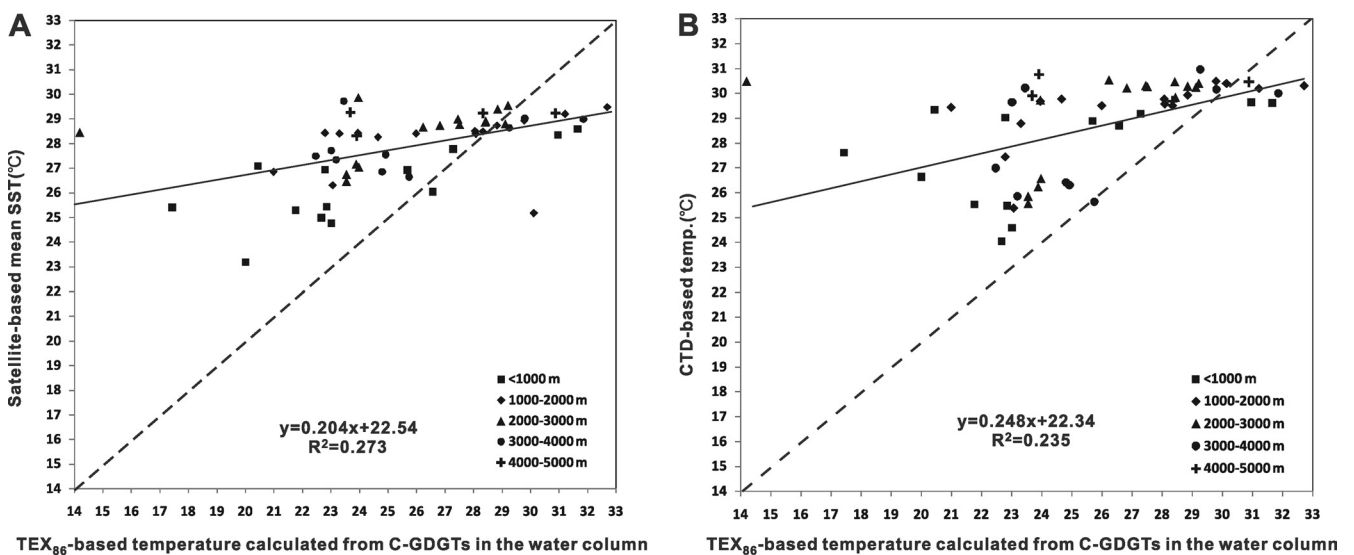

FIG. 6. (A) Correlations between satellite-based sea surface temperatures (from Fig. 5) and TEX$_{86}$-based temperatures (32). (B) Correlations between CTD *in situ* temperatures (from Fig. 5) and TEX$_{86}$-based temperatures (32). In both cases, the correlation is insignificant ($P > 0.05$).
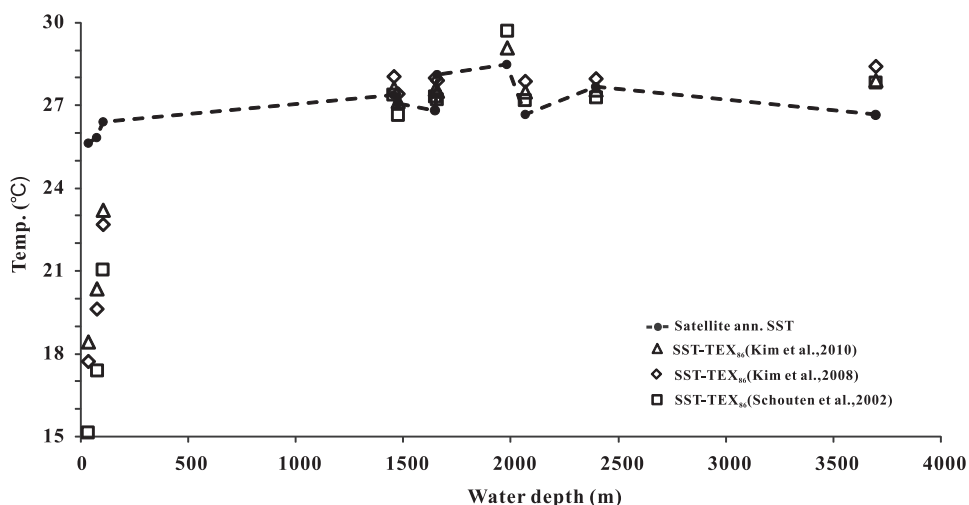
FIG. 7. Annual mean sea surface temperatures (satellite based) and TEX$_{86}$-derived temperatures for core-top sediment samples versus water depth.

Our observation of structural changes in CL and IPL (Table 2) agrees with a report for other marine sediments (42). However, Liu et al. (42) also showed significant correlations in the ring index and in the TEX$_{86}$-derived temperatures between C- and IP-GDGTs, which allowed them to explain the overall connections between these two lipid pools with three possibilities: (i) the pool of C-GDGTs is strongly influenced by sedimentary *in situ* production and subsequent hydrolysis of IP-GDGTs, (ii) the pool of IP-GDGTs largely represents molecular fossils derived from planktonic *Archaea*, and (iii) there is partial recycling by benthic *Archaea* of fossil C-GDGTs derived from planktonic *Archaea* (42). Neither our data nor those of Liu et al. (42) allow us to draw a conclusion about the exact sources of CL and IPL in the marine sediments. However, the lack of correlations in the ring index and in the TEX$_{86}$-derived temperatures between C- and IP-GDGTs in our study (data not shown) indicates the presence of other sources of C- and IP-GDGTs in the SCS sediments. Modeling (38, 39, 57) in combination with isotopic measurements of different intramolecular components of the GDGT molecules (37, 58, 60) and measurements of the metabolic status of *Archaea* (22, 24) may be needed to thoroughly evaluate to what extent the IP-GDGTs represent fossil or living archaeal biomass in natural environments.

TEX$_{86}$-derived temperatures. The development of the TEX$_{86}$ proxies has significantly advanced our understanding of paleoclimate change (12). In the core-top sediments, the TEX$_{86}$-derived temperatures based on the work of Kim et al. (32) agree with satellite-derived mean annual surface temperatures except for the shallow (<100-m) water depths, which show significantly lower temperatures than satellite values (Fig. 5). A similar discrepancy has been observed on the Italian shelf of the Gulf of Taranto by Leider et al. (35), who attributed the lower TEX$_{86}$-based temperatures for the near-shore sites to winter sea surface temperatures.

Studies of TEX$_{86}$ proxies in the water column, however, have resulted in ambiguous conclusions (53, 62). In this study, the satellite-derived as well as measured *in situ* temperatures were overall considerably higher than TEX$_{86}$-based tempera-

tures (Fig. 6). The central basin and the southern part of the SCS, however, show TEX$_{86}$-derived temperatures matching the satellite-derived or measured temperatures (Fig. 5), suggesting that planktonic *Archaea* produce GDGTs in response to sea surface temperature in these regions (G. Jia [personal communication], on the other hand, showed the best match between core-top TEX$_{86}$-derived temperatures with satellite-derived temperatures at water depths of 30 to 125 m in the SCS). The reasons for the considerably lower TEX$_{86}$ temperatures in other parts of the SCS are unknown, and sampling in other seasons is needed to better understand temporal responses of archaeal abundances and community structure to changes in sea surface temperatures. Changes in nutrients (62), transportation of exogenous cold-water-sourced particles (35), or hydrodynamics of the water column (34, 66) are possible reasons for the discrepancies between TEX$_{86}$-derived sea surface temperatures and measured temperatures.

Summary. A total of 57 surface water samples and 11 core-top sediment samples from the South China Sea were analyzed for the abundances of CL and IPL of *Archaea*. Because of the high sensitivity of the LC-MS (detection limit of 0.8 pg), we were able to measure low concentrations of CL (0.001 to 0.894 ng/liter) of *Archaea* in most of the filter samples. The distribution of the CL was heterogeneous, with high values occurring in regions where upwelling commonly occurs and low values occurring in the southeast area of the SCS. The CL of *Archaea* in surface marine sediments ranged from 0.11 μg/g to 0.90 μg/g, which were at the low end of CL concentrations commonly observed for other marine sediments and may reflect the oligotrophic productivity of the SCS. The IPL of *Archaea* represented 6 to 36.4% of total lipids (C plus IP), suggesting that the majority of archaeal lipids in core-top sediments were fossil remains of archaeal cells.

TEX$_{86}$-derived temperatures were best correlated to satellite-based or CTD-determined *in situ* temperatures when the formula most appropriate for nonpolar oceans was used (32). The TEX$_{86}$ temperatures for filter samples collected for the April-May season were better correlated to satellite mean surface temperatures for this season than for the mean annual sea
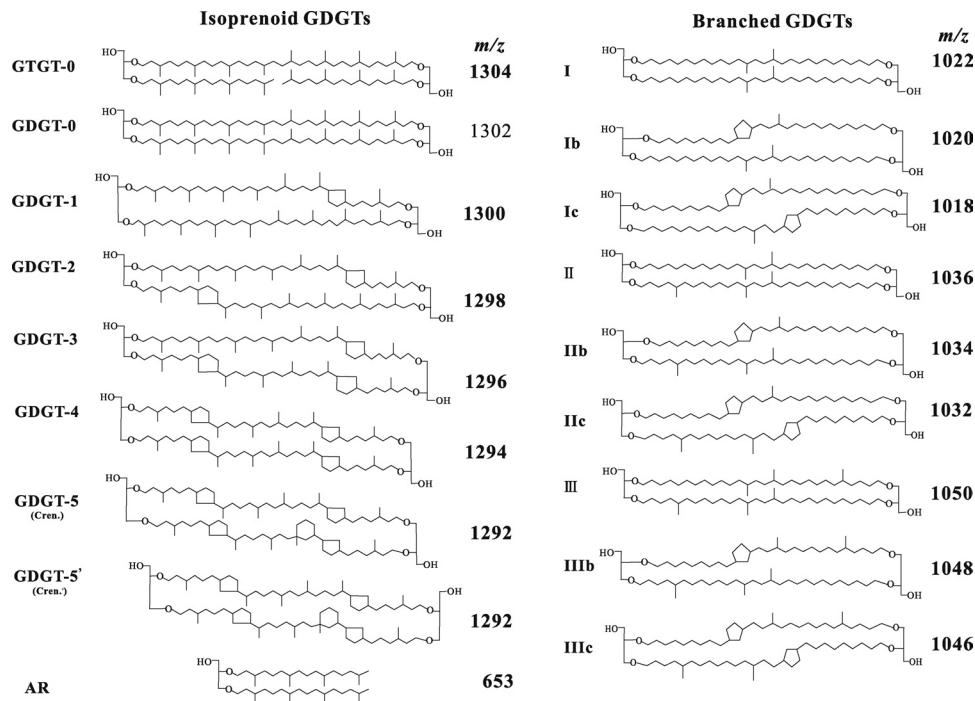
Isoprenoid GDGTs   **Branched GDGTs**

FIG. A1.

surface temperatures, suggesting that planktonic *Archaea* might respond to temperature variations at the seasonal scale. Nevertheless, the TEX_{86} temperatures of the surface water were significantly lower than satellite or CTD-derived temperatures; however, our data do not allow conclusions to be drawn about the causes of the discrepancies. TEX_{86} temperatures from surface marine sediments in the open ocean (water depth of >1,000 m) were within 1°C of the mean annual sea surface temperatures, suggesting the applicability of TEX_{86} proxies (32) for paleoclimate studies in at least the central basin of the South China Sea. The much lower TEX_{86} temperatures for marine sediments from depths shallower than 100 m indicated that caution must be exercised in interpretation of paleotemperatures from TEX_{86} values obtained from the shallow continental shelf of the SCS.

APPENDIX

Figure A1 shows the structures of isoprenoidal and branched glycerol dibiphytanyl glycerol tetraether (GDGT) and archaeol.

ACKNOWLEDGMENTS

REFERENCES

1. **Baltar, F., J. Aristegui, J. M. Gasol, S. Hernandez-Leon, and G. J. Herndl.** 2007. Strong coast-ocean and surface-depth gradients in prokaryotic assemblage structure and activity in a coastal transition zone region. Aquat. Microb. Ecol. **50:**63–74.
2. **Bard, E.** 2001. Comparison of alkenone estimates with other paleotemperature proxies. Geochem. Geophys. Geosyst. **2:**2000GC000050.
3. **Biddle, J. F., et al.** 2006. Heterotrophic *Archaea* dominate sedimentary subsurface ecosystems off Peru. Proc. Natl. Acad. Sci. U. S. A. **103:**3846–3851.
4. **Blaga, C., G.-J. Reichart, O. Heiri, and J. S. Sinninghe Damsté.** 2009. Tetraether membrane lipid distributions in water-column particulate matter and sediments: a study of 47 European lakes along a north-south transect. J. Paleolimnol. **41:**523–540.
5. **Bornemann, A., et al.** 2008. Isotopic evidence for glaciation during the Cretaceous supergreenhouse. Science **319:**189–192.
6. **Briggs, J. C.** 1999. Coincident biogeographic patterns: Indo-West Pacific Ocean. Evolution **53:**326–335.
7. **Castañeda, I. S., et al.** 2010. Millennial-scale sea surface temperature changes in the eastern Mediterranean (Nile River Delta region) over the last 27,000 years. Paleoceanography **25:**PA1208. doi:10.1029/2009PA001740.
8. **Chen, J. F., et al.** 1999. Vertical changes of POC flux and indicators of early degradation of organic matter in the South China Sea. Sci. China Ser. D Earth Sci. **42:**120–128.
9. **Church, M. J., et al.** 2003. Abundance and distribution of planktonic *Archaea* and *Bacteria* in the waters west of the Antarctic Peninsula. Limnol. Oceanogr. **48:**1893–1902.
10. **Coolen, M. J., et al.** 2007. Putative ammonia-oxidizing Crenarchaeota in suboxic waters of the Black Sea: a basin-wide ecological study using 16S ribosomal and functional genes and membrane lipids. Environ. Microbiol. **9:**1001–1016.
11. **Dumitrescu, M., S. C. Brassell, S. Schouten, E. C. Hopmans, and J. S. Sinninghe Damsté.** 2006. Instability in tropical Pacific sea-surface temperatures during the early Aptian. Geology **34:**833–836.
12. **Eglinton, T. I., and G. Eglinton.** 2008. Molecular proxies for paleoclimatology. Earth Planet. Sci. Lett. **275:**1–16.
13. **Francis, C. A., J. M. Beman, and M. M. Kuypers.** 2007. New processes and players in the nitrogen cycle: the microbial ecology of anaerobic and archaeal ammonia oxidation. ISME J. **1:**19–27.
14. **Galand, P. E., C. Gutiérrez-Provecho, R. Massana, J. M. Gasol, and E. O. Casamayor.** 2010. Inter-annual recurrence of archaeal assemblages in the coastal NW Mediterranean Sea (Blanes Bay Microbial Observatory). Limnol. Oceanogr. **55:**2117–2125.
15. **Gan, J. P., et al.** 2010. Biological response to intensified upwelling and to a river plume in the northeastern South China Sea: a modeling study. J. Geophys. Res. C Oceans **115:**C09001.

16. **Herfort, L., et al.** 2007. Variations in spatial and temporal distribution of *Archaea* in the North Sea in relation to environmental variables. FEMS Microbiol. Ecol. **62:**242–257.

17. **Hopmans, E. C., et al.** 2004. A novel proxy for terrestrial organic matter in sediments based on branched and isoprenoid tetraether lipids. Earth Planet. Sci. Lett. **224:**107–116.

18. **Hu, A., N. Jiao, and C. L. Zhang.** 20 May 2011. Community structure and function of planktonic Crenarchaeota: changes with depth in the South China Sea. Microb. Ecol. doi:10.1007/s00248-00011-09866-z.

19. **Huguet, C., et al.** 2008. Selective preservation of soil organic matter in oxidized marine sediments (Madeira Abyssal Plain). Geochim. Cosmochim. Acta **72:**6061–6068.

20. **Huguet, C., et al.** 2006. An improved method to determine the absolute abundance of glycerol dibiphytanyl glycerol tetraether lipids. Org. Geochem. **37:**1036–1041.

21. **Huguet, C., J. H. Kim, J. S. Sinninghe Damsté, and S. Schouten.** 2006. Reconstruction of sea surface temperature variations in the Arabian Sea over the last 23 kyr using organic proxies (TEX$_{86}$ and U$_{37}^{K'}$). Paleoceanography **21:**PA3003. doi:10.1029/2005PA001215.

22. **Huguet, C., W. Martens-Habbena, H. Urakawa, D. A. Stahl, and A. E. Ingalls.** 2010. Comparison of extraction methods for quantitative analysis of core and intact polar glycerol dialkyl glycerol tetraethers (GDGTs) in environmental samples. Limnol. Oceanogr. Methods **8:**127–145.

23. **Huguet, C., R. H. Smittenberg, W. Boer, J. S. Sinninghe Damsté, and S. Schouten.** 2007. Twentieth century proxy records of temperature and soil organic matter input in the Drammensfjord, southern Norway. Org. Geochem. **38:**1838–1849.

24. **Huguet, C., et al.** 2010. Changes in intact membrane lipid content of archaeal cells as an indication of metabolic status. Org. Geochem. **41:**930–934.

25. **Ingalls, A. E., et al.** 2006. Quantifying archaeal community autotrophy in the mesopelagic ocean using natural radiocarbon. Proc. Natl. Acad. Sci. U. S. A. **103:**6442–6447.

26. **Jia, G.-D., and P.-A. Peng.** 2003. Temporal and spatial variations in signatures of sedimented organic matter in Lingding Bay (Pearl estuary), southern China. Mar. Chem. **82:**47–54.

27. **Jian, Z., et al.** 2003. Pliocene-Pleistocene stable isotope and paleoceanographic changes in the northern South China Sea. Palaeogeogr. Palaeoclimatol. Palaeoecol. **193:**425–442.

28. **Jian, Z. M., B. H. Li, B. Q. Huang, and J. L. Wang.** 2000. Globorotalia truncatulinoides as indicator of upper-ocean thermal structure during the Quaternary: evidence from the South China Sea and Okinawa Trough. Palaeogeogr. Palaeoclimatol. Palaeoecol. **162:**287–298.

29. **Jing, Z.-Y., Y.-Q. Qi, Z.-L. Hua, and H. Zhang.** 2009. Numerical study on the summer upwelling system in the northern continental shelf of the South China Sea. Cont. Shelf Res. **29:**467–478.

30. **Karner, M. B., E. F. DeLong, and D. M. Karl.** 2001. Archaeal dominance in the mesopelagic zone of the Pacific Ocean. Nature **409:**507–510.

31. **Kim, J.-H., S. Schouten, E. C. Hopmans, B. Donner, and J. S. Sinninghe Damsté.** 2008. Global sediment core-top calibration of the TEX$_{86}$ paleothermometer in the ocean. Geochim. Cosmochim. Acta **72:**1154–1173.

32. **Kim, J.-H., et al.** 2010. New indices and calibrations derived from the distribution of crenarchaeal isoprenoid tetraether lipids: implications for past sea surface temperature reconstructions. Geochim. Cosmochim. Acta **74:** 4639–4654.

33. **Lam, P., et al.** 2007. Linking crenarchaeal and bacterial nitrification to anammox in the Black Sea. Proc. Natl. Acad. Sci. U. S. A. **104:**7104–7109.

34. **Lee, K. E., J. H. Kim, I. Wilke, P. Helmke, and S. Schouten.** 2008. A study of the alkenone, TEX$_{86}$, and planktonic foraminifera in the Benguela Upwelling System: implications for past sea surface temperature estimates. Geochem. Geophys. Geosyst. **9:**19.

35. **Leider, A., K.-U. Hinrichs, G. Mollenhauer, and G. J. M. Versteegh.** 2010. Core-top calibration of the lipid-based and TEX86 temperature proxies on the southern Italian shelf (SW Adriatic Sea, Gulf of Taranto). Earth Planet. Sci. Lett. **300:**112–124.

36. **Levipan, H. A., R. A. Quinones, and H. Urrutia.** 2007. A time series of prokaryote secondary production in the oxygen minimum zone of the Humboldt current system, off central Chile. Prog. Oceanogr. **75:**531–549.

37. **Lin, Y. S.** 2009. In vitro study of microbial carbon cycling in subseafloor sediments. Ph.D. thesis. Bremen University, Bremen, Germany.

38. **Lipp, J. S., and K. U. Hinrichs.** 2009. Structural diversity and fate of intact polar lipids in marine sediments. Geochim. Cosmochim. Acta **73:**6816–6833.

39. **Lipp, J. S., Y. Morono, F. Inagaki, and K. U. Hinrichs.** 2008. Significant contribution of *Archaea* to extant biomass in marine subsurface sediments. Nature **454:**991–994.

40. **Liu, B., et al.** 2009. Community structure of *Archaea* in the water column above gas hydrates in the Gulf of Mexico. Geomicrobiol. J. **26:**363–369.

41. **Liu, K. K., et al.** 2002. Monsoon-forced chlorophyll distribution and primary production in the South China Sea: observations and a numerical study. Deep Sea Res. Part I Oceanogr. Res. Pap. **49:**1387–1412.

42. **Liu, X., J. S. Lipp, and K.-U. Hinrichs.** 2011. Distribution of intact and core GDGTs in marine sediments. Org. Geochem. **42:**368–375.

43. **Liu, Z., et al.** 2009. Global cooling during the eocene-oligocene climate transition. Science **323:**1187–1190.

44. **Maindonald, J., and J. Braun.** 2003. Data analysis and graphics using R—an example based approach. Cambridge University Press, Cambridge, United Kingdom.

45. **Massana, R., A. E. Murray, C. M. Preston, and E. F. DeLong.** 1997. Vertical distribution and phylogenetic characterization of marine planktonic *Archaea* in the Santa Barbara Channel. Appl. Environ. Microbiol. **63:**50–56.

46. **Meyers, P. A.** 1997. Organic geochemical proxies of paleoceanographic, paleolimnologic, and paleoclimatic processes. Org. Geochem. **27:**213–250.

47. **Mincer, T. J., et al.** 2007. Quantitative distribution of presumptive archaeal and bacterial nitrifiers in Monterey Bay and the North Pacific Subtropical Gyre. Environ. Microbiol. **9:**1162–1175.

48. **Murray, A. E., et al.** 1998. Seasonal and spatial variability of bacterial and archaeal assemblages in the coastal waters near Anvers Island, Antarctica. Appl. Environ. Microbiol. **64:**2585–2595.

49. **Nicol, G. W., and C. Schleper.** 2006. Ammonia-oxidising Crenarchaeota: important players in the nitrogen cycle? Trends Microbiol. **14:**207–212.

50. **Pearson, A., et al.** 2004. Nonmarine crenarchaeol in Nevada hot springs. Appl. Environ. Microbiol. **70:**5229–5237.

51. **Powers, L., et al.** 2010. Applicability and calibration of the TEX$_{86}$ paleothermometer in lakes. Org. Geochem. **41:**404–413.

52. **Powers, L., et al.** 2004. Crenarchaeotal membrane lipids in lake sediments: a new paleotemperature proxy for continental paleoclimate reconstruction? Geology **32:**613–616.

53. **Schouten, S., et al.** 2008. Intact membrane lipids of "Candidatus Nitrosopumilus maritimus," a cultivated representative of the cosmopolitan mesophilic group I Crenarchaeota. Appl. Environ. Microbiol. **74:**2433–2440.

54. **Schouten, S., E. C. Hopmans, and J. S. Sinninghe Damsté.** 2004. The effect of maturity and depositional redox conditions on archaeal tetraether lipid palaeothermometry. Org. Geochem. **35:**567–571.

55. **Schouten, S., E. C. Hopmans, E. Schefuß, and J. S. Sinninghe Damsté.** 2002. Distributional variations in marine crenarchaeotal membrane lipids: a new tool for reconstructing ancient sea water temperatures? Earth Planet. Sci. Lett. **204:**265–274.

56. **Schouten, S., C. Huguet, E. C. Hopmans, and J. S. Sinninghe Damsté.** 2007. Improved analytical methodology of the TEX$_{86}$ paleothermometry by high performance liquid chromatography atmospheric pressure chemical ionization-mass spectrometry. Anal. Chem. **79:**2940–2944.

57. **Schouten, S., J. J. Middelburg, E. C. Hopmans, and J. S. Sinninghe Damsté.** 2010. Fossilization and degradation of intact polar lipids in deep subsurface sediments: a theoretical approach. Geochim. Cosmochim. Acta **74:**3806–3814.

58. **Shah, S. R., G. Mollenhauer, N. Ohkouchi, T. I. Eglinton, and A. Pearson.** 2008. Origins of archaeal tetraether lipids in sediments: insights from radiocarbon analysis. Geochim. Cosmochim. Acta **72:**4577–4594.

59. **Sinninghe Damsté, J. S., W. I. C. Rijpstra, and G.-J. Reichart.** 2002. The influence of oxic degradation on the sedimentary biomarker record. II. Evidence from Arabian Sea sediments. Geochim. Cosmochim. Acta **66:** 2737–2754.

60. **Takano, Y., et al.** 2010. Sedimentary membrane lipids recycled by deep-sea benthic *Archaea*. Nat. Geosci. **3:**858–861.

61. **Tamburini, F., T. Adatte, K. Föllmi, S. M. Bernasconi, and P. Steinmann.** 2003. Investigating the history of East Asian monsoon and climate during the last glacial-interglacial period (0-140 000 years): mineralogy and geochemistry of ODP sites 1143 and 1144, South China Sea. Mar. Geol. **201:**147–168.

62. **Turich, C., et al.** 2007. Lipids of marine *Archaea*: patterns and provenance in the water-column and sediments. Geochim. Cosmochim. Acta **71:**3272–3291.

63. **Wakeham, S. G., et al.** 2007. Microbial ecology of the stratified water column of the Black Sea as revealed by a comprehensive biomarker study. Org. Geochem. **38:**2070–2097.

64. **Wang, P., and Q. Li.** 2009. Developments in paleoenvironmental research, p. 1–12. *In* P. S. John (ed.), The South China Sea: paleoceanography and sedimentology, vol. 13. Springer, New York, NY.

64a.**Wang, P., et al.** 2010. Community structure of archaea from deep-sea sediments of the South China Sea. Microb. Ecol. **60:**796–806.

65. **Wuchter, C., S. Schouten, S. G. Wakeham, and J. S. Sinninghe Damsté.** 2006. Archaeal tetraether membrane lipid fluxes in the northeastern Pacific and the Arabian Sea: implications for TEX$_{86}$ paleothermometry. Paleoceanography **21:**PA4208. doi:10.1029/2006PA001279.

66. **Zhang, Y., et al.** 2009. Role of mesoscale cyclonic eddies in the distribution and activity of *Archaea* and Bacteria in the South China Sea. Aquat. Microb. Ecol. **56:**65–79.

67. **Zhao, M., C.-Y. Huang, C.-C. Wang, and G. Wei.** 2006. A millennial-scale U$_{37}^{K'}$ sea-surface temperature record from the South China Sea (8°) over the last 150 kyr: monsoon and sea-level influence. Palaeogeogr. Palaeoclimatol. Palaeoecol. **236:**39–55.